Nonsymmetric molecules driven by intense few-cycle laser pulses: Phase and orientation dependence of enhanced ionization

G. Lagmago Kamta[1,2] and A. D. Bandrauk[1]
[1]*Département de Chimie, Université de Sherbrooke, Sherbrooke, Québec, Canada, J1K 2R1*
[2]*Department of Medical Physics, McGill University, Montréal, Québec, Canada, H3G 1A4*
(Received 8 August 2007; published 13 November 2007)

The ionization of nonsymmetric heteronuclear diatomic molecules by intense few-cycle laser pulses linearly polarized along the internuclear axis has been investigated. It is found that enhanced ionization (EI) occurs in nonsymmetric molecules and is accompanied by enhanced excitation (EE). We show that the nonsymmetric distribution of the electron cloud between the two nuclei leads to a strong dependence of EI and EE on the carrier envelope phase of few-cycle pulses, and on the orientation of the molecule parallel or antiparallel with the peak electric field of the pulse. This effect is as strong as the pulse duration is short and disappears with increasing pulse duration. The field ionization model, and mainly the "energy level crossing" mechanism, are used to explain these phase effects. The newly proposed energy level crossing mechanism, which is relevant to nonsymmetric molecules, occurs as the driving field moves the dressed ground and excited states closer to each other until their energy levels cross, leading to an enhancement of excitation and ionization. A semiclassical nonadiabatic model derived to interpret the level crossing mechanism also predicts the critical internuclear distance R_c at which EI, EE, and energy crossings occur as a function of charge asymmetry and laser intensity, in good agreement with quantum-mechanical simulations.

DOI: 10.1103/PhysRevA.76.053409 PACS number(s): 33.80.Rv, 33.80.Eh, 33.80.Wz, 42.50.Hz

I. INTRODUCTION

The response of molecules to intense laser fields can be starkly different from that of atoms. The most conspicuous evidence of this is provided by the occurrence of enhanced ionization (EI) in molecules, which has been predicted for symmetric molecules and called charge resonance enhanced ionization (CREI) [1–5]. Experiments have confirmed these theoretical predictions of EI indirectly [6,7] and directly [8,9]. EI is the sharp increase in the ionization rate of molecules when they stretch to reach a critical internuclear distance R_c. Recent studies of symmetry effects on EI indicate that it may occur only in molecular systems in which the highest occupied molecular orbital is of σ type, i.e., with the electron cloud concentrated along the internuclear axis [10]. Although initially illustrated for symmetric diatomic molecules [1,2,4], EI has been observed in experiments involving complex molecules [11]. Furthermore, recent calculations suggest that EI also occurs in atomic clusters [12,13]. Therefore, the importance of EI extends well beyond the field of molecular physics.

Thanks to recent developments in laser technology, ultrashort optical laser pulses having as few as one oscillation cycle at the full width at half maximum (FWHM) can now be generated [14]. For such few cycle pulses, the electric field at the peak of the pulse depends strongly on the carrier-envelopE phase (CEP). An important advantage is that when subjected to such short pulses, atoms and molecules can experience the peak intensity of the pulse without being fully ionized, thereby increasing the possibility of a nonlinear electron response. In addition, few cycle pulses are short enough to resolve the fastest atomic motions, which means that such pulses could be used to take snapshots of nuclei in molecules while they undergo a given dynamic process such as Coulomb explosion [15].

Atoms and homonuclear (symmetric) molecules such as H_2, O_2, N_2, etc., are invariant under the space inversion symmetry, and the electron cloud is evenly distributed among the nuclei centers. As a consequence, when driven by a laser field, the total ionization probability of such molecular systems is unchanged when they undergo a space inversion. This remains true independently of the time duration and intensity of the laser pulse. In this work, we show that the situation is completely different for nonsymmetric molecules such as CO, HCl, HeH^+, etc., which are characterized by an electron cloud asymmetrically distributed among the nuclei, resulting in a molecule possessing a permanent dipole. It follows that orienting such a molecule such that the peak electric field of the laser pulse is parallel or antiparallel with the permanent dipole of the molecule (PDM) leads to different outcomes for EI. Preliminary results on this orientation dependence of EI have been discussed in Ref. [16] for HeH^{2+} molecule, which has been the subject of numerous experimental and theoretical research (see, e.g., Refs. [16–21], and references therein).

Our investigation focuses on the simplest case of a one electron diatomic heteronuclear nonsymmetric molecules (HeH^{2+}) driven by a few cycle pulses, because an exact numerical solution of the corresponding time-dependent Schrödinger equation (TDSE) is possible, within fixed nuclei and dipole approximations. This way we can investigate the strongly nonsymmetric molecule HeH^{2+}, but also, by assigning noninteger effective charges to the nuclei, we can approximately mimic more realistic diatomic molecular models for which the asymmetry in the electron cloud distribution is in general weaker than in HeH^{2+}. Our investigation shows that for nonsymmetric molecules, there is a strong dependence of EI on the CEP of few cycle pulses. This CEP sensitivity is as strong as the few cycle pulse is short and is essentially due to the nonsymmetric distribution of the elec-

tron cloud between the nuclei. We show that a key mechanism leading to the CEP sensitivity is the energy level crossing, which occurs in nonsymmetric molecules as the driving field moves the ground and excited states closer to each other, until an avoided energy crossing occurs.

This paper is organized as follows. In Sec. II, we describe the numerical approach used to solve the TDSE for an asymmetric diatomic molecule, as well as the corresponding stationary Schrödinger equation, which leads to electronic potential curves of molecules. The calculation of ionization and excitation probabilities is also discussed in Sec. II. Orienting HeH^{2+} (or equivalently adjusting the laser CEP) such that its permanent dipole is parallel or antiparallel with the laser peak electric field has a strong influence on the ionization and excitation of the molecule. These orientation effects are discussed in Sec. III, and the physical mechanisms responsible for these effects are investigated in Sec. IV. Section V is devoted to the study of the general influence of the laser CEP on EI. In Sec. VI, we discuss how the orientation and phase effects mentioned above are affected by the degree of asymmetry in molecules in general. A conclusion summarizes our results in Sec. VII. Unless otherwise stated, atomic units (a.u.) are used throughout this work.

II. SOLUTION OF SCHRÖDINGER EQUATIONS

A. The time-dependent Schrödinger equation

Assuming clamped nuclei, the TDSE for a one-electron diatomic molecule driven by a laser pulse is

$$i\frac{\partial}{\partial t}\Psi(\mathbf{r},t) = [H + \mathbf{A}(t,\phi)\cdot\mathbf{p}]\Psi(\mathbf{r},t), \tag{1}$$

where

$$H = \frac{\mathbf{p}^2}{2} - \frac{Z_1}{r_1} - \frac{Z_2}{r_2} \tag{2}$$

is the electronic Hamiltonian, $\mathbf{p}$ is the electron momentum, $\mathbf{r}$ is the electron distance relative to the geometric center of the nuclei, and $\mathbf{R}$ is the internuclear vector. $r_1 = |\mathbf{r}+\mathbf{R}/2|$ and $r_2 = |\mathbf{r}-\mathbf{R}/2|$ are the electron distances relative to the nuclei 1 and 2, respectively. The Coulomb potential experienced by the electron is

$$V(\mathbf{r}) = -Z_1/r_1 - Z_2/r_2, \tag{3}$$

where Z_1 and Z_2 are the electric charges of the nuclei 1 and 2, respectively. We make the following three choices that are convenient but do not impose any restriction on the system. (i) the z axis is along the internuclear axis of the molecule, (ii) the geometric center of the nuclei is taken as the origin of coordinates, (iii) $Z_1 \geq Z_2$; e.g., $Z_1=2$ and $Z_2=1$ for HeH^{2+}. Since $\mathbf{r}_1=\mathbf{r}+\mathbf{R}/2$ and $\mathbf{r}_2=\mathbf{r}-\mathbf{R}/2$, the choices (ii) and (iii) above indicate that the nucleus 1 (i.e., the most electronegative nucleus) is located on the negative side of the z axis. In more realistic molecular systems such as CO, HCl, …, etc., the charge asymmetry between the two centers is much less pronounced than in HeH^{2+}. In order to approximately incorporate this fact in our simulations, we will assume noninteger effective charges Z_1 and Z_2.

The laser pulse is linearly polarized along the molecular axis z, and its vector potential is given by $\mathbf{A}(t,\phi) = A_0 f(t)\sin(\omega t+\phi)\mathbf{e}_z$. Here A_0 is the maximum amplitude, ω is the laser frequency, ϕ is the CEP, and $\mathbf{e}_z$ is the unit vector along the laser's polarization axis. The envelope $f(t)$ of the pulse is a cosine squared given by

$$f(t) = \begin{cases} \cos^2(t/\tau) & \text{if } -\pi\tau/2 \leq t \leq \pi\tau/2, \\ 0 & \text{otherwise.} \end{cases} \tag{4}$$

The electric field of the laser pulse is derived from its potential vector $\mathbf{A}(t,\phi)$ as $\mathbf{E}(t,\phi) = -\frac{\partial \mathbf{A}}{\partial t}$, which ensures the zero area theorem for electromagnetic pulses. The laser-molecule interaction is described in the dipole approximation by the Hamiltonians $D_L = \mathbf{E}(t,\phi)\cdot\mathbf{r} = \mathbf{E}(t,\phi)z$ for the length gauge and by $D_V = \mathbf{A}(t,\phi)\cdot\mathbf{p} = \mathbf{A}(t,\phi)\frac{\partial}{\partial z}$ for the velocity gauge. The two gauges have been shown to agree well in the context of the basis expansion approach used in this work [22].

For a nonsymmetric molecule characterized by nuclei $Z_1 \neq Z_2$, the electron cloud is asymmetrically distributed between the nuclei. The corresponding electronic potential $V(\mathbf{r})$ is invariant under the transformations $x \to -x$ and $y \to -y$, but it is not invariant under the transformation $z \to -z$ along the molecular axis. Therefore, the Hamiltonian H in Eq. (2) is not invariant under the inversion symmetry transformation $\mathbf{r} \to -\mathbf{r}$, which means that parity is not a good quantum number. It follows that, in contrast to homonuclear molecules such as H_2 or H_2^+, the classification of the eigenstates of the system as gerade or ungerade is no longer valid. However, the projection L_z of the electronic angular momentum along the z axis is still conserved, since $[L_z, H]=0$. Thus in the absence of an external field, a nonsymmetric two-center molecule possesses an axial symmetry (z axis). In the presence of a laser field linearly polarized along the molecular axis z (as considered in this work), this axial symmetry is preserved, so that the field does not induce any change in the angular momentum projection m. It follows that in this case, the time-dependent wave function can be written as $\Psi(\mathbf{r},t) = \Psi^m(\mathbf{r},t)$, where m denotes initial state angular momentum projection along the z axis.

In order to solve the TDSE (1), we use spheroidal coordinates (ξ,η,φ), where $\xi=(r_1+r_2)/R$, $\eta=(r_1-r_2)/R$, and φ is the azimuthal angle. Expressions in spheroidal coordinates of the operators H, z and $\partial/\partial z$ can be found in Ref. [23]. We also expand the time-dependent wave function in a complex basis as

$$\Psi^m(\xi,\eta,t) = \sum_{\mu,\nu} a^m_{\mu\nu}(t) U^m_\nu(\xi) V^m_\mu(\eta) \frac{e^{im\phi}}{\sqrt{2\pi}}, \tag{5}$$

where $a^m_{\mu\nu}(t)$ are time-dependent coefficients and $U^m_\nu(\xi)$ and $V^m_\mu(\eta)$ are basis functions that depend on Laguerre and associated Legendre polynomials, respectively [22,24,25]. The integer indices μ and ν take the values $\mu = 0, 1, 2, \ldots, \mu_{\max}$; and $\nu = 0, 1, 2, \ldots, \nu_{\max}$. $\mu_{\max}$ and $\nu_{\max}$ determine the size of the basis. In principle, the accuracy of the results increases with increasing basis size (i.e., $\mu_{\max}$ and $\nu_{\max}$), and convergence of the results is achieved when they become unchanged by increasing $\mu_{\max}$ and $\nu_{\max}$.

Throughout this work, we deal with σ states ($m=0$). We use exterior complex scaling to prevent reflections of the electron probability flux at the boundaries of the region described by the wave function. Exterior complex scaling in spheroidal coordinates consists of making the transformation $(\xi,\eta,\varphi) \rightarrow (e^{-i\theta}\xi,\eta,\varphi)$ in the wave function $\Psi(\xi,\eta,\varphi)$ [26]. This is equivalent to having a complex nonlinear parameter $\beta = |\beta| e^{-i\theta}$ $(0<\theta<\pi/2)$, which makes the basis function $U_\nu(\xi)$ behave asymptotically as an outgoing wave [23].

A projection of the TDSE onto the basis expansion (5) leads to a system of first order differential equations

$$i\frac{\partial}{\partial t}\mathbf{S}\Psi = [\mathbf{H} + g(t)\mathbf{D}_z]\Psi, \tag{6}$$

where $\mathbf{S}$ and $\mathbf{H}$ denote the overlap and atomic Hamiltonian matrices, respectively. $g(t)$ is a scalar function that equals $E(t,\phi)$ for the length gauge and $-iA(t,\phi)$ for the velocity gauge. $\mathbf{D}_z$ is the matrix associated with the dipole operator z or ∂z, depending on the gauge used. Ψ is the vector representation of the wave function. Since we are dealing with laser fields linearly polarized along the internuclear axis z, the dipole operators lead to selection rules $\Delta m = m' - m = 0$, i.e., there are no dipole transitions between states with different electron angular momentum projection along the z axis.

The TDSE (6) is notoriously stiff [22], especially with increasing laser intensity and wavelength. The best way to tackle this system of differential equations is to use implicit methods, which are unconditionally stable [27], thereby allowing the use of relatively large integration steps. However, the price for this unconditional stability is that at each time step one has to invert matrices of the same size as those involved in Eq. (6). Explicit methods such as Runge-Kutta do not require such matrix inversions, but require only matrix-vector products instead. Unfortunately, the stability domain of explicit methods is much smaller than that of implicit methods. Moreover, with explicit methods, the stiffness of the TDSE (6) translates into the requirement for an increasingly smaller time step to maintain stability of the integration, even though accuracy requirements allow for a much larger time step [27]. With the very large size of matrices involved in Ref. [22] for homonuclear diatomic molecules at arbitrary orientation relative to the laser polarization axis, we found an explicit Runge-Kutta method to be more adequate. The reason for this is that due to the large matrices involved, the time cost of performing matrix inversions necessary for an implicit method surpasses that of performing the multiple matrix-vector products necessary for the explicit case. In addition, the fact that only gerade and ungerade states are coupled by the dipole in the homonuclear molecule case involved in Ref. [22] leads to much sparser matrices, which in turn leads to faster matrix-vector products with an appropriate algorithm. In the present work, we use a semi-implicit Rosenbrock method [27], as the selection rule $\Delta m = 0$ restricts the basis expansion (5) to a single m and leads to much smaller basis sizes than in Ref. [22], thereby permitting faster matrix inversions. The resulting extended stability allows us to deal with laser intensities as high as 10^{16} W/cm^2.

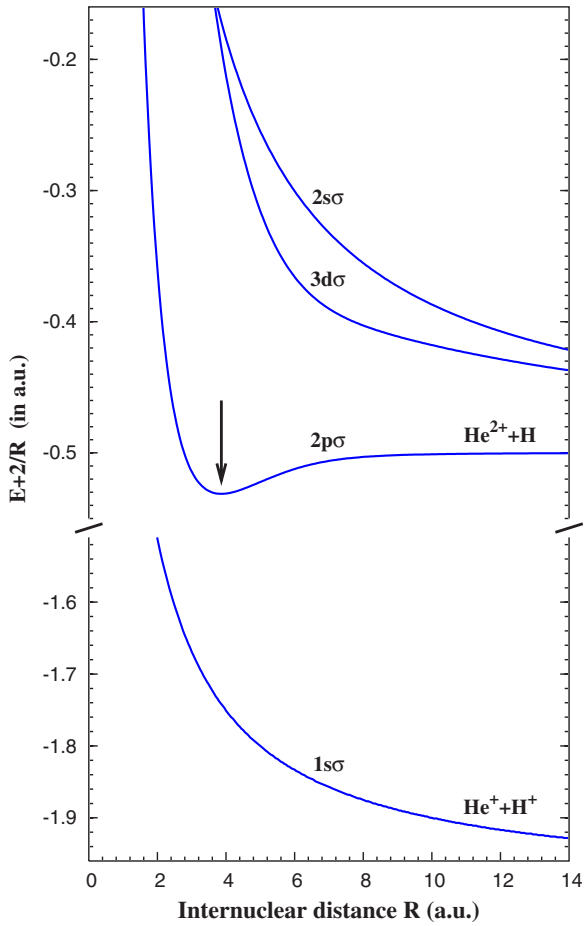

FIG. 1. (Color online) Potential curves for the lowest energy levels of HeH^{2+}. The minimum (indicated by the vertical arrow) at the internuclear distance $R_0=3.9$ a.u. for the $2p\sigma$ level indicates that this state is stable [28,29].

B. The stationary Schrödinger equation

The propagation of the TDSE requires the initial wave function $\Psi(\mathbf{r},t_{\text{ini}}) = \Phi_0(\mathbf{r})$, obtained by solving the stationary Schrödinger equation $H\Phi(\mathbf{r}) = E\Phi(\mathbf{r})$, which is equivalent with the expansion (5) to solving the generalized eigenvalue problem

$$\mathbf{H}\Phi = E\mathbf{S}\Phi. \tag{7}$$

The solution of this eigenvalue problem yields discrete electronic energies E_n and the corresponding wave functions Φ_n. These results are illustrated in Fig. 1, which shows the energies of few low-lying eigenstates of HeH^{2+} vs the internuclear distance R. Results are in very good agreement with *ab initio* potentials in Refs. [28,29]. In particular, we recover the attractive character of the first excited $2p\sigma$ state of HeH^{2+}, with its equilibrium internuclear distance at $3.89a_0$. Figure 1 also illustrates the repulsive character of the ground state $1s\sigma$ of HeH^{2+}. Note that with the electron in the $2p\sigma$, the molecule dissociates into a He^{2+} and H (corresponding to a

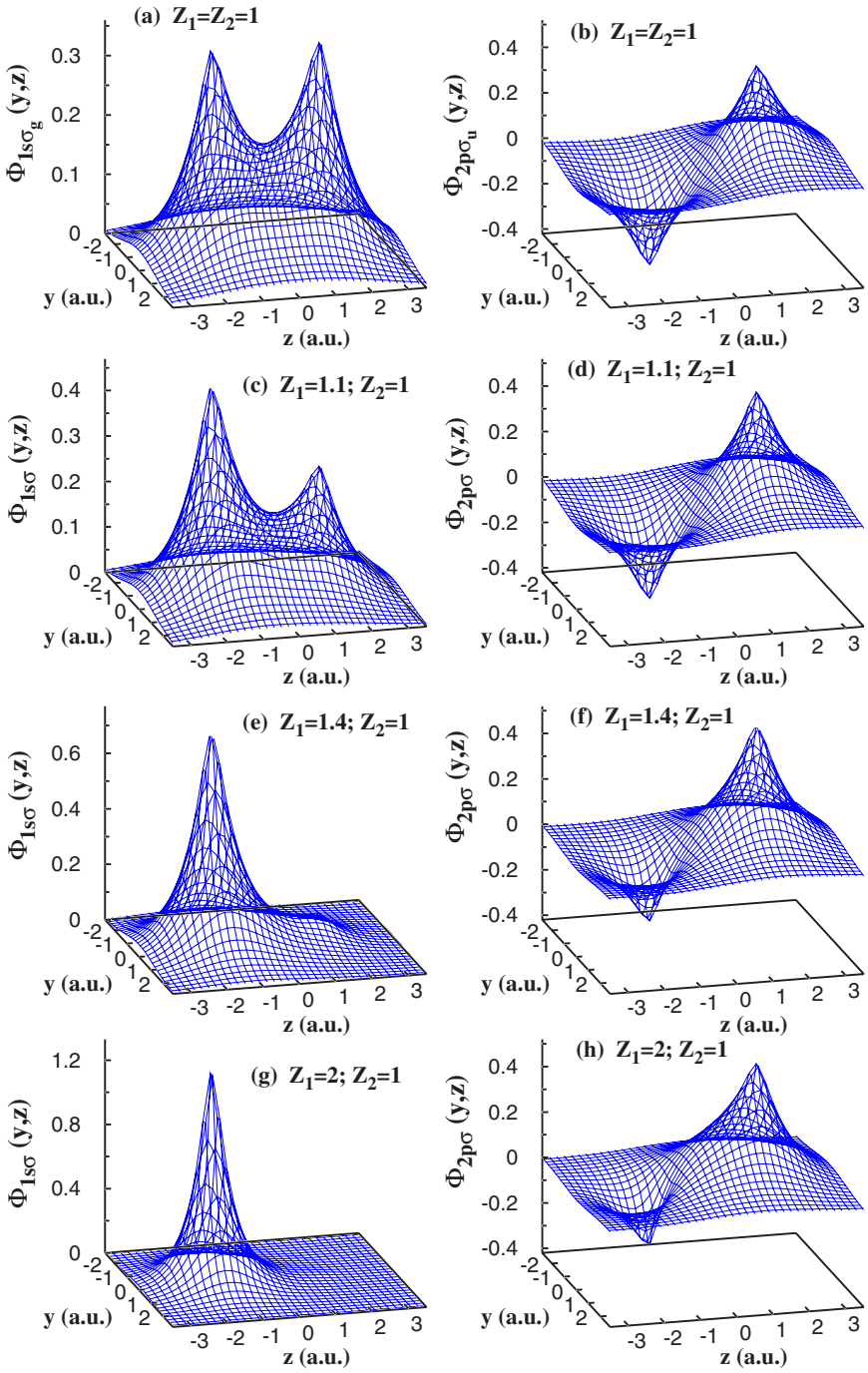

FIG. 2. (Color online) Wave functions of the ground state (left plots) and of the first excited state (right plots) of a one-electron diatomic molecule for various combinations of nuclear charges Z_1 and Z_2. (a) and (b) $1s\sigma_g$ and $1s\sigma_u$ states of H_2^+ for $Z_1=Z_2=1$; (c) and (d) $1s\sigma$ and $2p\sigma$ states for $Z_1=1.1$ and $Z_2=1$; (e) and (f) $1s\sigma$ and $2p\sigma$ states for $Z_1=1.4$ and $Z_2=1$; (g) and (h) $1s\sigma$ and $1s\sigma$ states of HeH^{2+} for $Z_1=2$ and $Z_2=1$. In all cases $R=3$ a.u. The nuclei are located along the z axis at $z=\pm R/2$.

charge transfer), whereas with the electron in the $1s\sigma$, the molecule dissociates into a He^+ and H^+. This kind of asymmetry in the dissociation product is expected to occur in all nonsymmetric molecules.

To illustrate the asymmetry (relative to the plane perpendicular to the z axis at its origin) in the electron cloud distribution characterizing nonsymmetric molecules, we plot in Fig. 2 the wave functions Φ of the two lowest eigenstates for various effective nuclear charges $Z_1=1$, $Z_1=1.1$, $Z_1=1.4$, and $Z_1=2$, for fixed $Z_2=1$ and $R=3a_0$. Note that fractional charges can be the result of electron transfer in molecular systems. The two lowest states $1s\sigma_g$ and $1s\sigma_u$ of H_2^+ plotted, respectively, in Figs. 2(a) and 2(b), illustrate a symmetric electron distribution between the nuclei centers. For the case $Z_1=1.1$ and $Z_2=1$ in Figs. 2(c) and 2(d), the rather small difference between Z_1 and Z_2 translates into a breakdown of the inversion symmetry along the z axis, and one sees that the electron cloud is no longer symmetrically distributed among the two nuclei. Figure 2 clearly shows that this asymmetry in the electron distribution increases with the difference Z_1-Z_2 in nuclear charges between the two centers. Note also that for ground-state wave functions $1s\sigma$ plotted on the left in Fig. 2 [i.e., Figs. 2(c), 2(e), and 2(g)], the electron cloud is increasingly localized on the most electronegative nucleus located on the left (i.e., on the nucleus with the largest effective charge) as the charge asymmetry between the nuclei increases. The same situation occurs for the first excited state $2p\sigma$, but here the electron is increasingly localized

on the right, around the nucleus with the smallest electric charge.

A further analysis of wave functions indicates that with increasing internuclear distance R (for fixed nuclear charges Z_1 and Z_2), the electron in the ground state is increasingly localized on the nucleus with the largest charge, whereas for the first excited state the electron is increasingly localized on the nucleus with the smallest charge. This corroborates the results in Fig. 1 for HeH^{2+} that in the dissociating limit, the $1s\sigma$ state leads to $He^+ + H^+$ whereas the $2p\sigma$ state leads to $He^{2+} + H$.

C. Ionization and excitation probabilities

Electronic states Φ_n having negative energies ($E_n < 0$) obtained from solving Eq. (7) are located below the ionization threshold and correspond to "bound" electronic states, and positive energy states ($E_n > 0$) correspond to discretized continuum states. The total ionization probability at the end of laser pulse is

$$P_{\text{ion}} = 1 - \sum_{n(E_n<0)} |\langle \Phi_n | \Psi(t_{\text{end}}) \rangle|^2, \tag{8}$$

where $\Psi(t_{\text{end}})$ is the time-dependent wave function at the end of the laser pulse, and where the summation runs over all "bound" states. The excitation probability P_{exc}, i.e., the probability for finding the system in all excited states is obtained as the probability for finding the system at the end of the laser pulse in all "bound" states except the initial state, i.e.,

$$P_{\text{exc}} = \sum_{n(E_n<0)} |\langle \Phi_n | \Psi(t_{\text{end}}) \rangle|^2 - |\langle \Phi_0 | \Psi(t_{\text{end}}) \rangle|^2. \tag{9}$$

Typical basis parameters used in our time-dependent calculations are $\mu_{\max}=35$ and $\nu_{\max}=80$, which corresponds to 2916 basis functions. The nonlinear parameter is $\beta=0.2$, and the complex rotation angle is $\theta=0.1$. Our results are fully converged, as they are almost insensitive to a change in basis parameters. The initial state for time propagation is considered throughout this work as the ground state $1s\sigma$.

III. ORIENTATION EFFECTS IN ENHANCED IONIZATION AND EXCITATION

In the interaction of a nonsymmetric molecule with a few cycle pulse linearly polarized along the molecular axis, there are two possible orientations for the molecule. The molecule could be oriented such that its permanent dipole is antiparallel (i.e., the A orientation) with the electric field at the peak of the few cycle pulse as shown in Fig. 3(a), or parallel (i.e., the P orientation) as in Fig. 3(b). In this section, we focus on the influence of these two orientations on the ionization of HeH^{2+}. Note that for atoms and molecules, which are inversion symmetric and which do not possess a permanent dipole, the ionization is unchanged when the system is rotated by 180°, independently of the laser intensity, pulse duration, and frequency.

Figure 4 shows results obtained using a three cycle pulse of frequency $\omega_0=0.114$ a.u. (400 nm), with a time duration of 1.5 laser periods (or laser cycles) at the FWHM, which

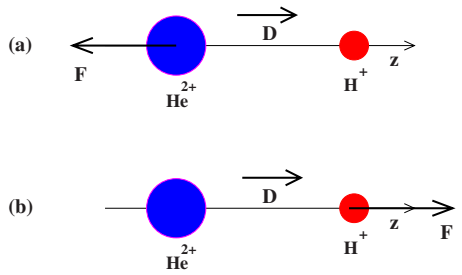

FIG. 3. (Color online) The two configurations along which a nonsymmetric molecule (e.g., HeH^{2+}) can be aligned relative to a static electric field **F**. The direction of the permanent dipole **D** of the molecule is also shown. (a) The A orientation; (b) the P orientation.

corresponds to a total duration of 4 fs. The electric field $E(t,\phi)$ of this laser pulse for the peak intensity 5×10^{15} is illustrated in Fig. 4(a) for the two CEPs $\phi=0$ and $\phi=\pi$. Note that changing the phase from $\phi=0$ to $\phi=\pi$ (and vice versa) is equivalent to changing the sign of the electric field of the laser pulse. Also, for the CEP $\phi=0$ the electric field at the peak of the pulse is negative and is therefore antiparallel with the dipole moment [see, e.g., Fig. 3(a)], whereas for $\phi=\pi$ the peak electric field is positive and parallel to the dipole moment [see, e.g., Fig. 3(b)].

The ionization probability of HeH^{2+} vs the internuclear distance R is plotted in Figs. 4(b)–4(d), respectively, for the laser peak intensities 5×10^{15}, 3×10^{15}, and 10^{15} W/cm^2. In all cases, the laser pulse duration and frequency used are the same as in Fig. 4(a). In this figure and in subsequent ones, dots are the calculated data, and lines are just drawn to guide the eye. For each intensity, the ionization probability is plotted for the two CEPs $\phi=0$ and $\phi=\pi$. It appears that EI occurs in all cases shown, as the ionization probability undergoes a sharp increase when some critical internuclear distance is reached (i.e., about 3, 4, and 5 a.u. for peak intensities 5×10^{15} W/cm^2, 3×10^{15} W/cm^2, and 10^{15} W/cm^2, respectively). In other words, the critical internuclear distance R_c at which EI is maximum decreases with increasing laser peak intensity. Another interesting feature that arises from Fig. 4 is the fact that EI is much stronger for $\phi=0$ than for $\phi=\pi$, independently of the peak intensity of the laser. Since changing the phase from $\phi=0$ to $\phi=\pi$ (and vice versa) is equivalent to rotating the molecule by 180°, this asymmetry in EI is not only a phase effect, but also an orientation effect.

The excitation probability in Fig. 5 shows features similar to those of the ionization probability in Figs. 4(b)–4(d): the excitation probability is enhanced approximately at the same critical internuclear distance R_c as the ionization probability in Fig. 4, and this R_c also tends to decrease with increasing laser peak intensity. Another similarity with the ionization probability in Fig. 4 is that the excitation probability is stronger for $\phi=0$ than for $\phi=\pi$. This means that EI is accompanied by enhanced excitation (EE) of the molecule.

Figure 6 shows the R dependence of the ionization probability of HeH^{2+} driven by laser fields with the same peak intensity 5×10^{15} W/cm^2, but having increasing time dura-

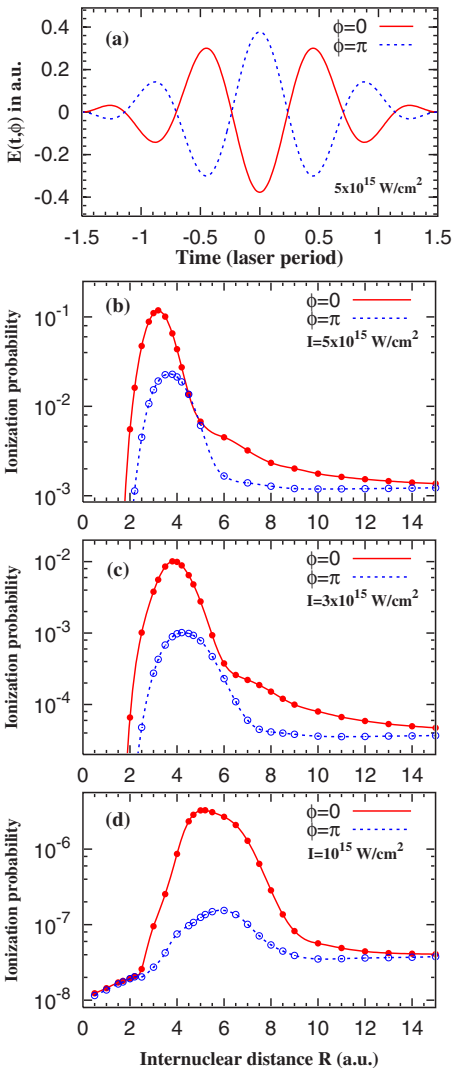

FIG. 4. (Color online) (a) Electric field $E(t,\phi)$ of a laser pulse for $\phi=0$ and $\phi=\pi$. The pulse has a cosine square envelope, a frequency $\omega_0=0.114$ a.u. (400 nm), a total pulse duration of three laser cycles, and a peak intensity $I=5\times10^{15}$ W/cm^2. Time is given in units of the laser cycle (i.e., laser period) $T_0=2\pi/\omega_0=1.3$ fs. The ionization probability of HeH^{2+} by laser pulses with CEPs $\phi=0$ and $\phi=\pi$ are plotted for various peak intensities: (b) $I=5\times10^{15}$ W/cm^2; (c) $I=3\times10^{15}$ W/cm^2; (d) $I=10^{15}$ W/cm^2.

tions. The ionization probability shown on each right plot of this figure is obtained with the laser pulse plotted on the corresponding left plot. One sees that the critical internuclear distance at which EI occurs is independent of the laser pulse duration, and that the asymmetry (i.e., $\phi=0$ vs $\phi=\pi$) in EI is as strong as the pulse duration is short. The strength of this EI asymmetry decreases with increasing laser pulse duration and becomes negligible when the laser pulse contains more than about six laser cycles (14 fs). In particular, Fig. 6(b) indicates that for an incident half cycle pulse with a positive electric field (i.e., and electric field parallel to the PDM) no EI occurs, whereas it occurs strongly for a half-cycle pulse with a negative electric field [see solid lines in Fig. 6(b)] which is antiparallel to the PDM. This suggests that EI is almost entirely induced by a half cycle with a negative electric field (i.e., antiparallel with the PDM).

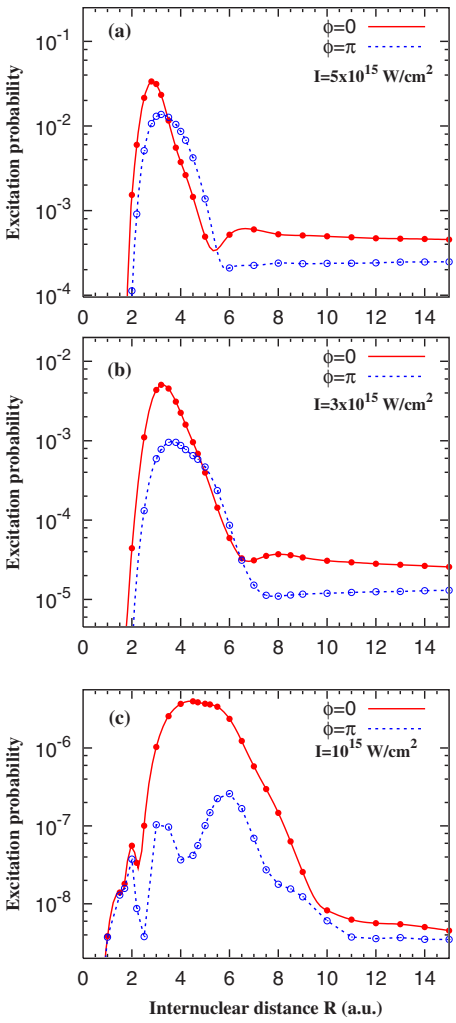

FIG. 5. (Color online) Total excitation probability for HeH^{2+} for the same laser frequency and pulse durations as in Fig. 4(a). The same peak intensities as in Fig. 4 are considered: (a) $I=5\times10^{15}$ W/cm^2; (b) $I=3\times10^{15}$ W/cm^2; (c) $I=10^{15}$ W/cm^2. For each intensity, results for the two CEPs $\phi=0$ and $\phi=\pi$ are shown.

Adding a period to this half-cycle pulse leads the pulse in Fig. 6(c), and the corresponding ionization probability in Fig. 6(d) clearly shows not only a strong EI for $\phi=0$ as expected, but also an onset of EI peak for $\phi=\pi$. This feature, superimposed with results in Fig. 6(b) for a half-cycle pulse, also indicates that the occurrence of EI in Fig. 6(d) for $\phi=\pi$ is due to the presence of two half-cycles with a negative electric field in the corresponding pulse [dashed lines in Fig. 6(c)]: one near the turn-on and the other near the turn-off of the pulse. However, as shown in Fig. 6(d), the $\phi=0$ orientation (for which the peak electric field is negative) leads to a much stronger EI than the $\phi=\pi$ orientation for which the peak electric field is positive. With increasing pulse duration [see Figs. 6(e) and 6(g)], the $\phi=0$ case still dominates [see Figs. 6(f) and 6(h)], but the strength of the asymmetry in EI decreases rapidly. In other words, the asymmetry in EI decreases with increasing pulse duration. The reason is that by increasing the number of oscillations in the pulse, one also increases the number of half-cycles with a negative electric field of the $\phi=\pi$ pulse, which boosts EI and thereby allows

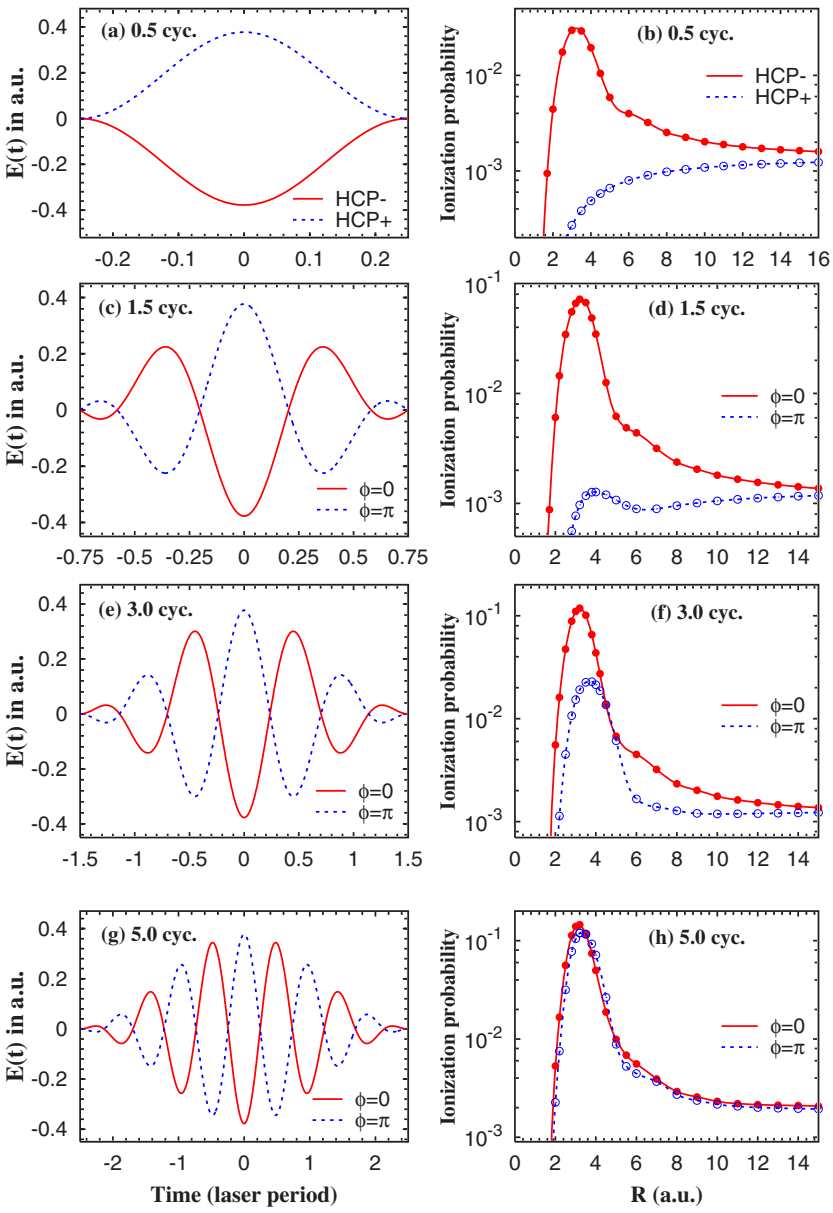

FIG. 6. (Color online) Influence of the laser pulse duration on the orientation asymmetry ($\phi=0$ vs $\phi=\pi$) in the enhanced ionization of HeH^{2+}. Right plots show the R dependence the ionization probability obtained with laser pulses whose electric fields are shown on the left. In all cases, the frequency is $\omega_0=0.114$ a.u. and the peak intensity is $I=5\times10^{15}$ W cm^2. The total durations of these pulses are 0.67 fs for the half-cycle in (a); 2.0 fs (1.5 cycles) for (c); 4.0 fs (3.0 cycles) for (e); 6.66 fs (5.0 cycles) for (g).

EI for $\phi=\pi$ to "catch up" on the EI for $\phi=0$.

A similar pattern is found for the excitation probability shown in Fig. 7, where a strong EI is obtained using a half-cycle pulse with the electric field oriented antiparallel to the PDM ($\phi=0$), whereas there is no EE obtained with a half-cycle pulse having an electric field parallel to the PDM ($\phi=\pi$). Also, for the same reasons as above for EI, this figure illustrates the decreasing EE with the laser pulse duration. It appears from the above results and discussions that EI is always accompanied by EE, and that the orientation asymmetry in EI and in EE decreases with the laser pulse time duration. In the next section, we investigate the mechanisms responsible for this asymmetry in EI and EE.

IV. MECHANISMS RESPONSIBLE FOR ASYMMETRIES IN EI AND EE

The results discussed in the previous section suggest that a half cycle with a negative electric field (i.e., a field that is antiparallel to the PDM) is almost entirely responsible for the occurrence of enhanced ionization. Therefore, investigating the interaction of the molecule with a static electric field having the same sign and intensity as the half-cycle would help uncover the mechanism behind the EI and EE asymmetries. To explain the asymmetry in EI, we study HeH^{2+} in a static field $\vec{F}$, which can be oriented parallel (P) or antiparallel (A) with the PDM. Using the complex basis (5), we diagonalize the Hamiltonian

$$H_S = H + Fz \tag{10}$$

of the system in the static field $\vec{F}=F\vec{e}_z$, for the two possible orientations $F>0$ (i.e., the P orientation) and $F<0$ (i.e., the A orientation). The resulting eigenvalues (the so-called quasienergies) are complex: their real parts are the energies of the system dressed by the field and their imaginary parts are the ionization rates of the corresponding states in the static field [30].

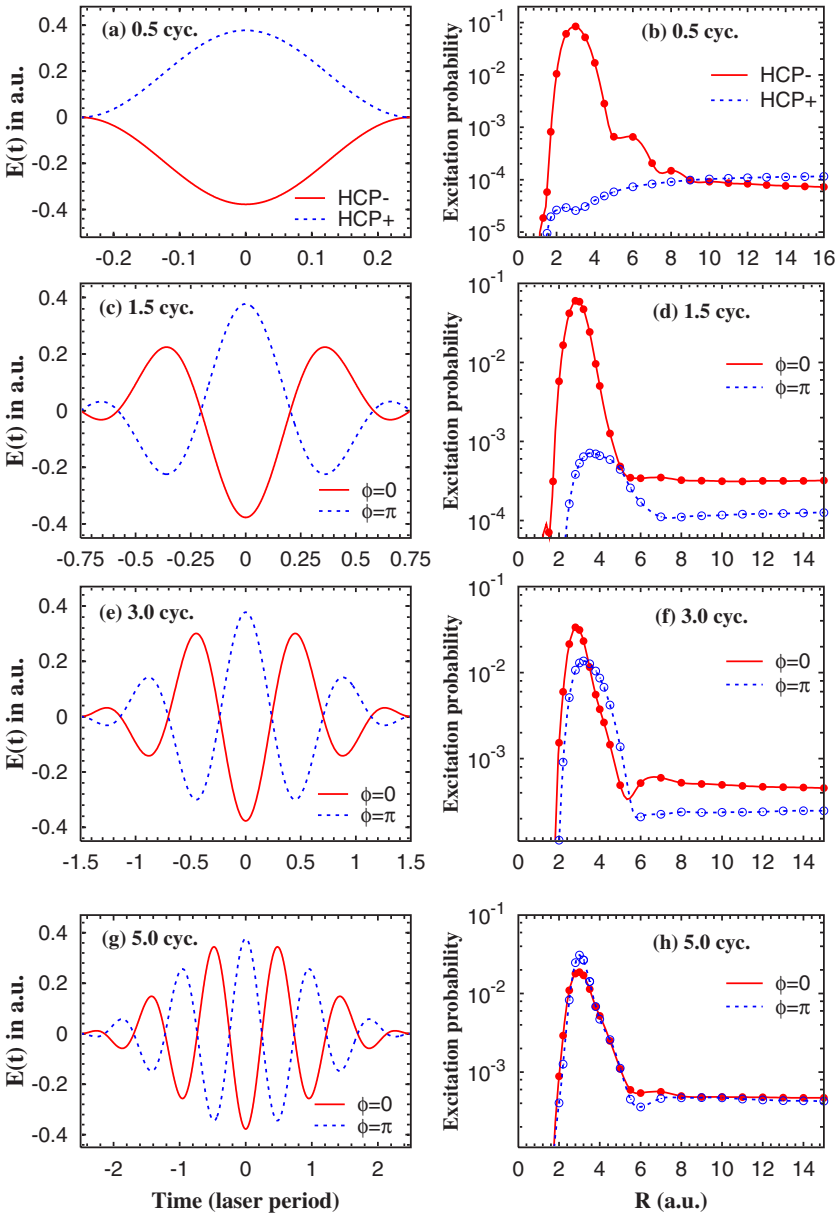

FIG. 7. (Color online) Same as Fig. 6 with identical laser parameters, but with right plots showing the excitation probability.

A. The field ionization mechanism

A tunnel ionization based interpretation for the asymmetry in EI illustrated in Figs. 4 and 6 can be provided by the so-called field ionization model, which has been used to explain EI for the case of homonuclear molecules [1–4]. For this purpose we plot in Fig. 8 a restriction along the z axis of the combined Coulomb potential $V(\mathbf{r})$ added to the molecule-static field interaction Hamiltonian Fz. For each internuclear distance selected, we show results for $F<0$ (A orientation) on the left column, and those for $F>0$ (P orientation) on the right column. Needless to say, for homonuclear molecules the left and right plots in Fig. 8 would be identical. We have also shown in this figure the energies of the two lowest dressed states $1s\sigma^*$ and $2p\sigma^*$ of HeH^{2+}. Note that the star in the exponent is added to indicate that we refer to corresponding states in the presence of the external static field, i.e., energies of these states are eigenvalues of the Hamiltonian in Eq. (10).

For the small internuclear distances illustrated in Figs. 8(a) and 8(b), the ground-state $1s\sigma^*$ energy level is deep in the potential, but well above the maximum of the inner barrier between the two wells. Needless to say, excited states are also well above this inner barrier between the two wells. Therefore, the ground state, as well as excited states effectively experience a single well potential. It follows that for such small internuclear distance, the ionization is atomiclike and identical for the A and P orientations of the molecule.

As the nuclei move apart, the static field acts over a larger distance and is more effective in lowering or raising the potential barrier (via Fz coupling). At some critical internuclear distance R_c the ionization rate of the molecule is enhanced because the electron can tunnel across or escape above the narrow inner barrier [1–3] into the continuum [see, e.g., Figs. 8(c) and 8(d)]. Even if the ground-state level is not above the inner potential barrier between the two wells, a strong coupling of the ground state with excited states in higher levels populates the latter [see, e.g., Figs. 8(d)], and thus provides

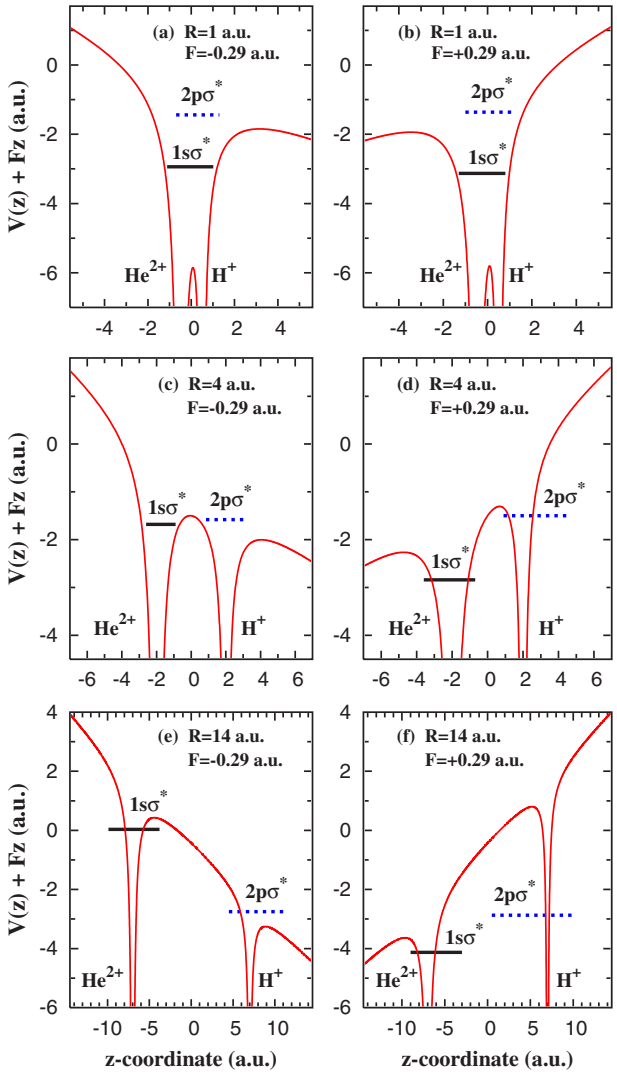

FIG. 8. (Color online) Restriction along the internuclear axis z of the combined Coulomb and static field potentials $V(\mathbf{r})+Fz$ of HeH^{2+}, for various R's ($R=1$, 4, and 14 a.u.) and for various orientations of an external static field $\vec{F}=F\vec{e}_z$ of strength $|F|=0.29$ a.u. ($I=3\times10^{15}$ W/cm^2). Left plots correspond to the A orientation ($F<0$) and right plots to the P orientation ($F>0$). Energy levels of the field-dressed $1s\sigma^*$ (solid lines) and $2p\sigma^*$ (dashed lines) states are shown.

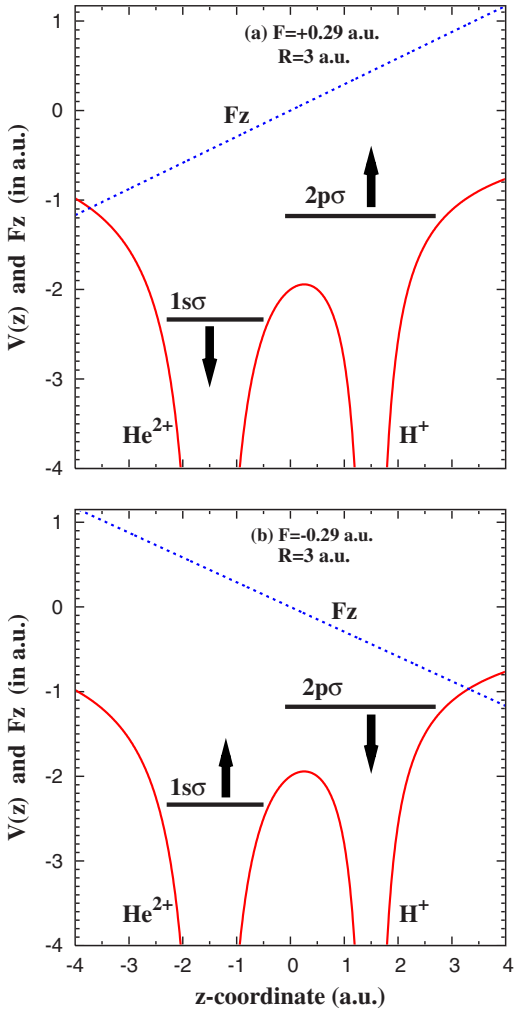

FIG. 9. (Color online) Coulomb potential $V(z)$ for a diatomic nonsymmetric molecule (e.g., HeH^{2+}) along the internuclear axis z (solid line) and the Hamiltonian Fz (dashed lines) of the interaction of the electron with the static field $\vec{F}=F\vec{e}_z$: (a) $F=+0.29$ a.u. corresponds to $\vec{F}$ parallel to the permanent dipole of the molecule (PDM); (b) $F=-0.29$ a.u. corresponds to $\vec{F}$ antiparallel with the PDM. The energy levels of the field-free states $1s\sigma$ and $2p\sigma$ are indicated with horizontal lines. The arrows indicate the displacement of the two energy levels by the applied field $\vec{F}$.

an indirect and easier path into the continuum via tunneling through the narrow inner barrier from the populated excited states [1]. This mechanism occurs at some intermediate internuclear distance R_c and is well established as the main mechanism for enhanced ionization in homonuclear molecules [1–3].

This mechanism also occurs at a critical internuclear distance in our nonsymmetric case for both A and P orientations of the molecule, justifying the occurrence of EI in each case. However, a characteristic feature for nonsymmetric molecules is that the electron cloud is asymmetrically distributed among the nuclei. As illustrated in Fig. 2, the electron cloud in the $1s\sigma$ state is localized on the He^{2+} nucleus (left potential well in Figs. 8 and 9), whereas the electron cloud in the $2p\sigma$ state is localized on the proton (right potential well in Figs. 8 and 9). For the A orientation ($F<0$), increasing $|F|$ or R raises energy level of the left localized ground-state electron, while lowering the right potential barrier [see Fig. 9(b)]; thus the electron can tunnel through or escape above the narrow internuclear potential straight into the continuum [see Fig. 8(c)], thereby boosting the ionization rate. In contrast, for the P orientation ($F>0$) the energy level of the left localized ground-state electron is lowered while the right potential barrier is raised [Fig. 9(a)]. Here ionization is hindered because the electron has to tunnel through a much wider left potential barrier to reach the continuum [see Fig. 8(d)]. This provides a first explanation of stronger EI for the A orientation than for the P orientation, and consequently provides a justification for a stronger ionization probability for $\phi=0$ than for $\phi=\pi$.

As ions further move apart beyond the critical internuclear distance R_c [see, e.g., Figs. 8(e) and 8(f)], electrons are increasingly localized on one or the other ions as the inner barrier between the two wells raises and widens. This suppresses tunneling between the two wells, and with the decreasing influence of the Coulomb field of each nucleus on the electron in the neighboring well, the ionization rate of the molecule decreases at $R > R_c$. Thus for $R \gg R_c$, the ionization rate becomes atomiclike and identical for $F < 0$ and $F > 0$.

B. The energy crossings (avoided) mechanism

The field ionization mechanism described in Sec. IV A does not explain the fact that EI is accompanied by a strong EE illustrated in Figs. 5 and 7 for various intensities and pulse durations. In particular, this mechanism does not explain the strong EI and EE observed for negative half-cycle pulses in Figs. 6(b) and 7(b), which contrasts with the absence of EI and EE for the positive HCP in the same figures. This suggests the contribution of another mechanism in addition to field ionization, which we discuss below.

Before investigating this mechanism, let us recall that the Coulomb potential experienced by the electron due to the two asymmetric nuclei is nonsymmetric with respect to the plane that intersects perpendicularly with the internuclear axis at the geometric center of the molecule. It follows an asymmetric distribution of the electron cloud between the nuclei along the molecular axis. Figure 9 shows a restriction along the molecular axis z of the Coulomb potential $V(\mathbf{r})$ [given by Eq. (3)] experienced by the electron, as well as the Hamiltonian Fz for the interaction of the electron with a static field. The electron cloud in the $1s\sigma$ state is predominantly localized around the He^{2+} nucleus on the left in Fig. 9, and this localization on He^{2+} is increasingly pronounced as the internuclear distance increases. In contrast, the $2p\sigma$ electron is increasingly localized around the proton on the right plots in Fig. 9, as the internuclear distance increases. Figure 9(a) for the P orientation ($F > 0$) clearly indicates that with increasing R or with increasing $|F|$, the influence of the static field is to move the lowest and left localized level $1s\sigma$ down, while moving the highest and right localized level $2p\sigma$ up, so that the two levels never cross each other. In contrast, for the A orientation ($F < 0$) illustrated in Fig. 9(b), the action of the static field is to move the ground level $1s\sigma$ up, while bringing the excited level $2p\sigma$ down, so that a crossing eventually occurs with increasing R or with increasing $|F|$. Note that the occurrence of this crossing requires that in the absence of external field, the two lowest levels of the nonsymmetric molecule be predominantly localized in different wells. In other words, the two levels involved must not be degenerate in the dissociating limit.

This picture is corroborated by quantum-mechanical calculations in which we have computed the energies for the two lowest $1s\sigma^*$ and $2p\sigma^*$ states of HeH^{2+} dressed by the static field $\vec{F}$, for various R values. The resulting potential curves (i.e., the eigenvalues of the Hamiltonian H_S in Eq. (10) vs R for the two dressed states $1s\sigma^*$ and $2p\sigma^*$ are plotted in Fig. 10 for the A orientation ($F < 0$), and for various values of the field strength $|F|$. All plots in Fig. 10 indicate

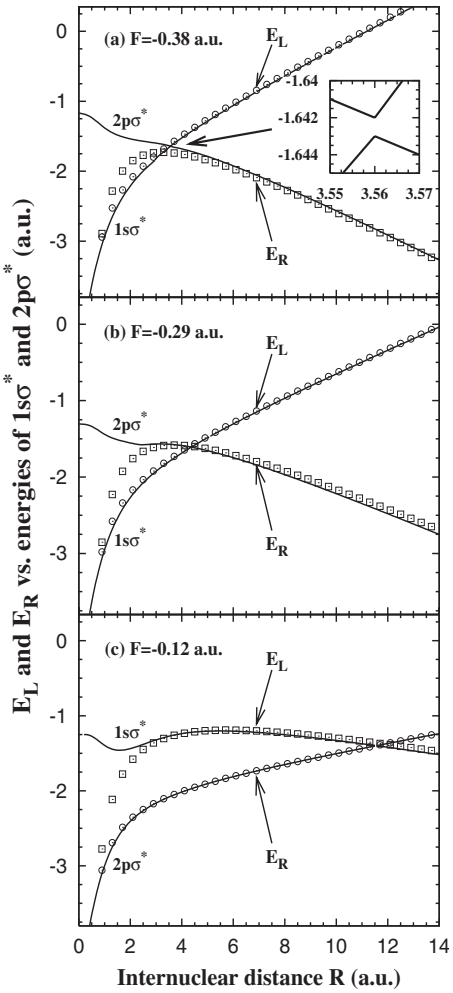

FIG. 10. Solid lines show energies of $1s\sigma^*$ and $2p\sigma^*$ states of HeH^{2+} dressed by a static field $\vec{F}=F\vec{e}_z$ for negative field (i.e., $F < 0$ or $\vec{F}$ antiparallel to the PDM) shown: (a) $F=-0.38$ a.u. (5×10^{15} W/cm^2), where the inset is a zoom illustrating the avoided crossing at R_{cros} between the two energy levels; (b) $F=-0.29$ a.u. (3×10^{15} W/cm^2); (c) $F=-0.12$ a.u. (5×10^{14} W/cm^2). The left and right energies given by Eqs. (11) and (12) are represented by circles and squares, respectively.

that with increasing R, the energy of the dressed ground state $1s\sigma^*$ is lifted up and undergoes an avoided crossing with the energy of the first excited state which is moving down. Another important feature is that the internuclear distances at which these avoided crossings occur increase with decreasing field strength (the same pattern as EE and EI discussed in the previous sections). In all cases these are truly avoided crossings, as illustrated in the inset of Fig. 10(a), which is a zoom in the vicinity of the crossing between the two energy levels. In contrast, for the P orientation ($F > 0$), the energy of the dressed ground state $1s\sigma^*$ moves downward with increasing R, so that there is no crossing with excited states.

The avoided crossings involving the ground state $1s\sigma^*$ in Fig. 10 appear to have a stronger influence (compared with the field ionization mechanism discussed in Sec. IV A) on the asymmetries in EI and EE displayed in Figs. 4–7. Indeed, the fact that the ground state moves up to undergo an

avoided crossing with excited states strengthens the coupling between the ground state and these excited states by the field, resulting in an enhancement of the excitation probability (see Figs. 5 and 7), as more population is easily pumped into excited states. This enhancement of the excitation probability is also due to the fact that fewer photon transitions are necessary to transfer population from the ground state to excited states near the avoided crossing. These strongly populated excited states are closer to the ionization threshold than the ground state, so that ionization is much easier via tunneling or multiphoton processes. In other words, the avoided crossings of the ground state with excited states for the A orientation enhance the ionization rates via a two step mechanism: (a) population of excited states and (b) tunnel and/or multiphoton ionization from these excited states. For the P orientation where the ground state moves away from excited states with increasing R, the absence of this two step mechanism leads to an absence of EI and EI for the half-cycle pulses in Figs. 6(b) and 7(b), respectively. For more conventional laser pulses EI and EE are stronger for $\phi=0$ than for $\phi=\pi$ [see Figs. 4(b)–4(d), 5, 6(c)–6(h), and 7(c)–7(h)], thanks to the absence of this two-step mechanism at the peak of electric field for $\phi=\pi$ (the corresponding peak half cycle corresponds to $F>0$ or P orientation). As discussed earlier, with increasing pulse duration, more and more half-cycles corresponding to the A orientation occur in the pulse, thereby allowing the ionization for $\phi=0$ and $\phi=\pi$ to coalesce.

We now attempt to derive an approximate analytical formula for the internuclear distance R_{cros} at which the crossings between the two lowest levels are expected to occur, using an approach similar to one used previously for homonuclear molecules for over-barrier ionization [4]. Our derivation is based on two assumptions. (i) In the dissociating limit (asymptotically large R), the energies of the two crossing levels are nondegenerate. These energies tend to the ionization potentials of the residual atoms or ions in which the electron is left. (ii) R_{cros} is large enough that it is fairly accurate to say that the electron in each of the two crossing levels is localized predominantly on one of the two wells. Indeed, for small internuclear distances as illustrated in Figs. 8(a) and 8(b), the inner electronic potential barrier is so far below the low lying states that the assumption (ii) that electrons are predominantly localized in left or right potential wells is no longer invalid.

As illustrated in Fig. 1, with increasing R the $1s\sigma$ energy level tends to the ionization potential $-I_1=-Z_1^2/2$ of He^+, whereas the $2p\sigma$ energy level tends to the ionization potential $-I_2=-Z_2^2/2$ of H. If the assumption (ii) is valid, then the field-free energy of the electron in the left well ($1s\sigma$ state) in Fig. 9(b) is approximately $-I_1-Z_2/R$, where $-Z_2/R$ is the Coulomb attraction due to the neighboring ion H^+. In the presence of the static field $F<0$, the energy of the electron in this left well is lifted up by $|F|R/2$ to become

$$E_L=-I_1-Z_2/R+|F|R/2. \tag{11}$$

Using a similar approach, one can show that the energy of the electron in the right well [$2p\sigma$ state in Fig. 9(b)] in the presence of the static field $F<0$ is approximately given by

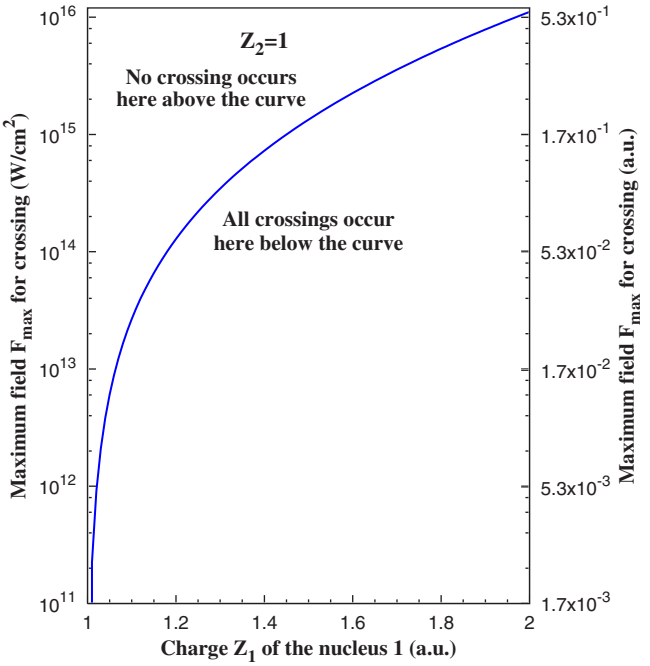

FIG. 11. (Color online) Magnitude of the static field F_{max} (the corresponding intensity is shown in W/cm^2 on the right side of the vertical axis) above which no crossing occurs between the two lowest levels of a nonsymmetric diatomic molecule vs the electric charges Z_1 and Z_2 of the nuclei (here, $Z_2=1$). According to the nonadiabatic model, level crossings occur only for molecule and laser parameters below the curve.

$$E_R=-I_2-Z_1/R-|F|R/2. \tag{12}$$

We shall discuss the accuracy of formulas (11) and (12) later. A level crossing occurs when $E_L=E_R$, i.e., when

$$|F|R^2-(I_1-I_2)R+(Z_1-Z_2)=0. \tag{13}$$

As expected, this equation is meaningful only if $Z_1\neq Z_2$ (i.e., for nonsymmetric molecules). In addition, Eq. (13) has real (physical) solutions if

$$\frac{(I_1-I_2)^2}{Z_1-Z_2}\geq 4|F| \tag{14}$$

or, equivalently, if (using $I_j=Z_j^2/2$, $j=1,2$)

$$(Z_1-Z_2)(Z_1+Z_2)^2\geq 16|F|. \tag{15}$$

This indicates that for a diatomic molecule with nuclear charges Z_1 and Z_2 there is a field magnitude $|F\mathrm{max}|=(Z1-Z2)(Z1+Z2)2/16$ above which no energy crossing occurs even if $F<0$. Figure 11 shows $|F_{\mathrm{max}}|$ for various values of Z_1, with a fixed $Z_2=1$. It appears that the larger the charge asymmetry in the molecule, the larger is $|F_{\mathrm{max}}|$.

When the conditions in Eq. (14) or (15) is satisfied, then Eq. (13) has two mathematical solutions $R_{\pm}=[(I_1-I_2)\pm\sqrt{(I_1-I_2)^2-4|F|(Z_1-Z_2)}]/2|F|$, which are plotted in Fig. 12. As shown in Fig. 12, the solution R_- leads to internuclear distances smaller than 1 a.u., which violates the assumption (ii). In other words, the molecule is atomiclike for such small internuclear distances [see, e.g., Figs. 8(a) and

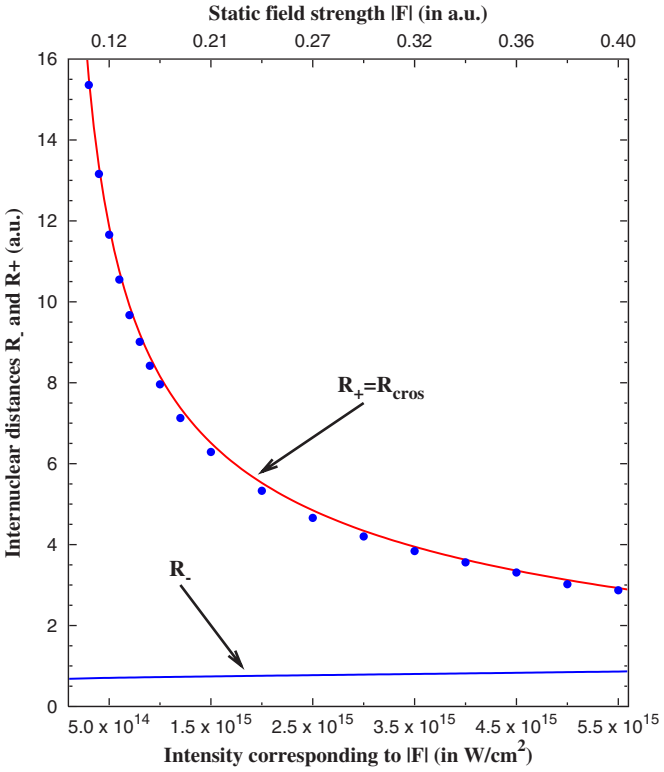

FIG. 12. (Color online) Mathematical solutions R_- and R_+ of the quadratic Eq. (13), vs the static field strength $|F|$. The only physical solution $R_+ \equiv R_{\text{cros}}$ given by Eq. (16) is the internuclear distance at which a crossing between the two lowest energy levels of HeH^{2+} occurs. The solution R_- is unphysical because it leads to very small internuclear distances, for which the two wells of the diatomic molecule coalesce into a single well. Dots are the quantum-mechanical values of R_{cros} obtained from the eigenvalues of the dressed Hamiltonian H_S in Eq. (10).

8(b)]; thus the concepts of left- and right-localized electrons leading to Eqs. (11) and (12) are completely meaningless. Therefore, we discard R_- and retain only the larger R_+ solution as the physically acceptable internuclear distance at which crossings are expected to occur, i.e.,

$$R_{\text{cros}} \equiv R_+ = \frac{(I_1 - I_2) + \sqrt{(I_1 - I_2)^2 - 4|F|(Z_1 - Z_2)}}{(2|F|)}. \quad (16)$$

Note that the above equation was misprinted in Ref. [16] without the exponent 2 in the first term in the square root. Equation (16) indicates that R_{cros} decreases with increasing field strength $|F|$, and eventually violates the condition (ii) when $|F|$ becomes larger than $F_{\max}$. Finally, it is clear again from Eq. (16) that these crossings occur only in nonsymmetric molecules for which $I_1 \neq I_2$ and $Z_1 \neq Z_2$.

The quantum-mechanical values of internuclear distances R_{cros} at which energy crossings occur [obtained from the eigenvalues of Eq. (10)] are compared with the predictions of Eq. (16) in Fig. 12. One sees that the Eq. (16) agrees well with quantum-mechanical results over a wide range of intensities. It appears that the internuclear distance at which crossings occur increases with decreasing laser intensity similarly to EI and EE, which supports our interpretation that these crossings are responsible for EI and EE as illustrated in Figs. 4–7. As a matter of fact, the internuclear distances R_c at which EI and EE are maximum are very close to R_{cros}.

The good agreement between the values of R_{cros} obtained from Eq. (16) and from quantum-mechanical calculations already provides insight into the accuracy of the approximate formulas (11) and (12). We further illustrate this accuracy in Fig. 10, where we plot the potential curves for the dressed $1s\sigma^*$ and $2p\sigma^*$ against the left and right energies given by Eqs. (11) and (12). One sees that at small internuclear distances for which the molecule is atomiclike, Eqs. (11) and (12) are quite inaccurate. This is expected because in this case the condition (ii) is not satisfied. However, with increasing R, for which the condition (ii) holds, the left energy E_L in Eq. (11) agrees very well with the energy of the left localized $1s\sigma^*$ state of HeH^{2+}, while the right energy E_R in Eq. (12) agrees with the energy of the right localized $2p\sigma^*$ state of HeH^{2+}.

V. INFLUENCE OF THE CARRIER-ENVELOPE PHASE

So far, we have discussed the asymmetry in enhanced ionization for the P and A orientations of the molecule, which correspond only to the two carrier envelop phases $\phi = 0$ and $\phi = \pi$, respectively. In this section, we perform a more extensive analysis of the influence of the laser CEP on EI. Results are summarized in Fig. 13 where EI for HeH^{2+} is shown for various pulse durations and for CEPs $\phi = 0$, $\phi = \pi/2$, $\phi = \pi$, and $\phi = 3\pi/2$.

The much stronger EI for the CEP $\phi = 0$ relative to $\phi = \pi$ has been shown in previous sections to be due to a negative peak electric field in the pulse for $\phi = 0$, as opposed to a positive peak electric field for $\phi = \pi$. These two CEPs lead to the maximum magnitude for the peak electric field achievable for a given pulse duration, a maximum that occurs at the center of the pulse. Thus, as illustrated in Figs. 13(a) and 13(c), the maximum peak electric field achieved in the pulse for other CEPs is lower in magnitude compared to $\phi = 0$ and $\phi = \pi$. Therefore the strongest EI is obtained for $\phi = 0$ and the weakest EI for $\phi = \pi$ [see in Figs. 13(b) and 13(d)], for a given pulse duration.

Let us now consider results for the two pairs of CEPs $\phi = \pi/2$ and $\phi = 3\pi/2$ which are also a phase π apart. This is a quite interesting case, because for each CEP the corresponding electric field [see Figs. 13(a) and 13(c)] has two dominant peaks with the same absolute magnitude; one negative and the other positive. The only difference between $\phi = \pi/2$ and $\phi = 3\pi/2$ is the timing of occurrence of the negative and positive peak half-cycles. Yet, substantial differences in EI are seen in the results, where the ionization rate is much stronger for $\phi = \pi/2$ than for $\phi = 3\pi/2$. For $\phi = 3\pi/2$, the first maximum of the electric field is positive, i.e., it corresponds to a positive half-cycle which leads to very negligible EI and EE, as discussed previously. During the next half-cycle the electric field is negative, leading to a strong EI and EE. However, for the $\phi = \pi/2$, the first maximum of the electric field is negative, leading to a strong EI due to the field ionization mechanism and mostly the energy crossing mechanism, which strongly populates excited states.

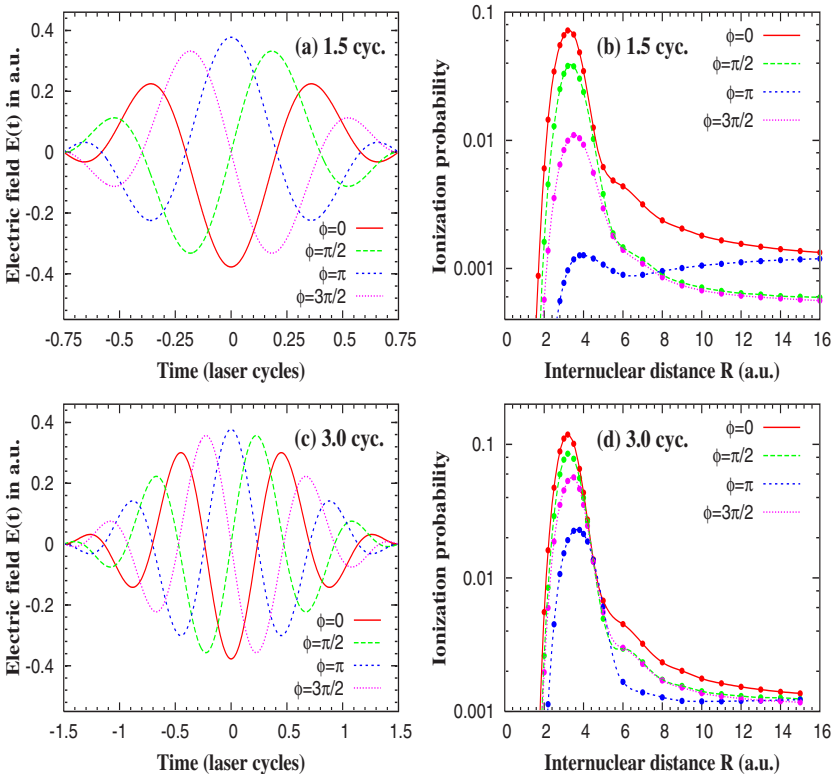

FIG. 13. (Color online) The electric field for various CEPs ϕ are shown in the left plots for total pulse durations of 1.5 and 3.0 laser cycles (cyc.), i.e., (a) for 1.5 cyc.; (c) for 3.0 cyc. The ionization probability of HeH^{2+} vs R is shown on the right plots for the laser pulses on the left: (b) and (d). In all cases, the laser peak intensity is 5×10^{15} W/cm^2 and the frequency is $\omega=0.114$ a.u.

The next peak of the electric field is positive and corresponds to a positive half-cycle, which in this case (and in contrast to the $\phi=3\pi/2$ case) also yield significant ionization arising from excited states (easier to ionize via tunneling or multiphoton processes) generated during the first peak of the electric field. This results in a stronger EI for $\phi=\pi/2$ than for $\phi=3\pi/2$, a feature that is sustained for various pulse durations [see Figs. 13(c) and 13(d)].

Note also that with increasing internuclear distances, as the electron becomes increasingly located on one nucleus, the molecule becomes atomiclike, leading to identical ionization rates for a 180° rotation of the molecule, i.e., results for $\phi=0$ are identical to $\phi=\pi$ at large R, and similarly for $\phi=\pi/2$ and $\phi=3\pi/2$. Furthermore, as expected, the phase dependence of EI increasingly disappears with increasing pulse duration (see Fig. 13).

VI. INFLUENCE OF THE NONSYMMETRIC ELECTRON DISTRIBUTION

Due to the strong charge asymmetry Z_1-Z_2 between the nuclei in HeH^{2+}, the Coulomb repulsion between the two nuclei makes this molecule unstable in its ground state. Therefore, it is not a realistic representation of stable nonsymmetric molecules which are potentially good candidates for experiments, and which have a much weaker charge asymmetry. However, such molecules can be simulated in the first approximation by adjusting effective charges Z_1 and Z_2 on each nucleus, to reproduce the lower effective charge asymmetry of nonsymmetric two-center molecules. In this section we investigate the influence of the charge asymmetry Z_1-Z_2 on the phase dependence of EI illustrated in previous sections.

Results are summarized in Fig. 14 for the two CEPs $\phi=0$ vs $\phi=\pi$, where the ionization probability for a diatomic molecule vs internuclear distance R is shown for increasing charge asymmetry between the two nuclei, starting from the H_2^+ case ($Z_1=Z_2=1$). These results indicate that except for the homonuclear molecule case in Fig. 14(a) where identical results are obtained for the two CEPs, there is a strong phase dependence of EI on the nuclear charge asymmetry Z_1-Z_2. Identical results for $\phi=0$ and $\phi=\pi$ is expected, as a 180° rotation of the homonuclear molecule leaves ionization unchanged. Therefore, the asymmetry in EI for $\phi=0$ vs $\phi=\pi$ is solely due to charge asymmetry between the nuclei.

Note, however, that for a charge asymmetry as small as 10% in Fig. 14(b) (i.e., $Z_1=1.1$ and $Z_2=1$), results show a significant phase dependence of EI. This clearly suggests that the dependence of EI on CEP can be expected in more stable nonsymmetric molecules (which are also most possible candidates for experiments) which have a weaker nuclei charge asymmetry than HeH^{2+}, such as alkali-metal hydrides LiH^+ and halogen compounds such as HCl^+ [31]. In general, Fig. 14 illustrates that the asymmetry in EI for $\phi=0$ vs $\phi=\pi$ increases with increasing charge asymmetry Z_1-Z_2, with stronger EI for $\phi=0$ as found for HeH^{2+}.

VII. SUMMARY AND CONCLUSIONS

Using an *ab initio* approach involving the solution of the three-dimensional time-dependent Schrödinger equation for diatomic molecules interacting with intense ultrashort laser pulses, we have shown that heteronuclear (nonsymmetric) molecules exhibit a strong sensitivity of EI on the laser CEP, a sensitivity that is absent in homonuclear (symmetric) mol-

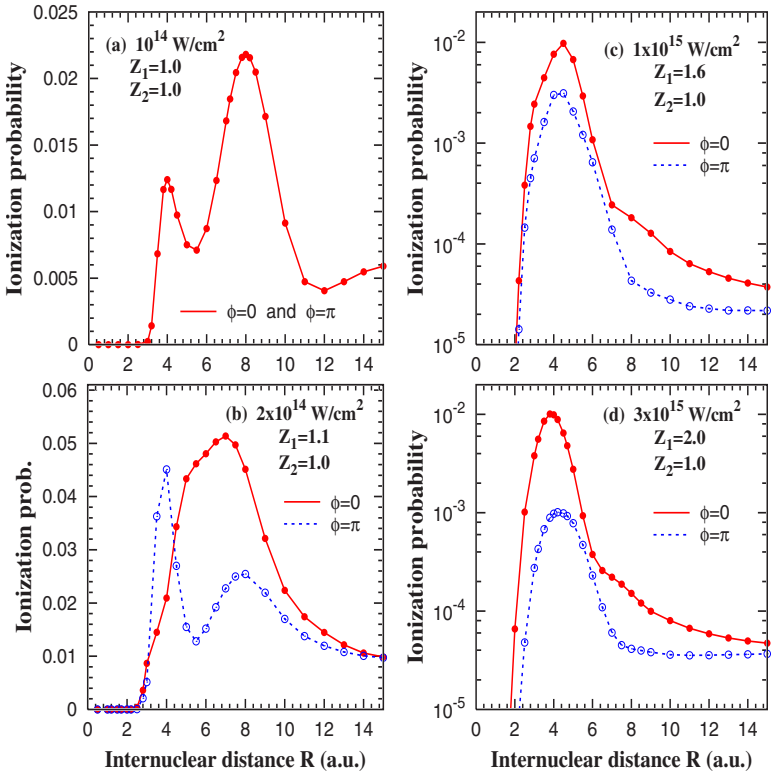

FIG. 14. (Color online) Phase dependence of EI for various charge asymmetries between the two nuclei: (a) for $Z_1=Z_2=1$; (b) for $Z_1=1.1$ and $Z_2=1$; (c) for $Z_1=1.6$ and $Z_2=1$; (d) for $Z_1=2$ and $Z_2=1$. In each case, two molecular orientations (i.e., two CEPs $\phi=0$ and $\phi=\pi$) are considered. The laser pulse used in all cases has a frequency $\omega=0.114$ a.u., and a total duration of three laser cycles.

ecules. Our investigation first focused on HeH^{2+} with two CEPs $\phi=0$ (for which the peak electric field of the pulse is antiparallel with the dipole of the molecule) and $\phi=\pi$ (for which peak electric field is parallel with the dipole). EI is found to be substantially stronger in general for $\phi=0$ than for $\phi=\pi$, and to be accompanied by a strong EE. This EI asymmetry ($\phi=0$ vs $\phi=\pi$) is shown to be solely due to the nonsymmetric distribution of the electron cloud among the nuclei. We also show that in addition to the field ionization mechanism, the level crossing mechanism contribute strongly to this EI asymmetry ($\phi=0$ vs $\phi=\pi$). The level crossing mechanism is proposed as a new physical mechanism relevant to nonsymmetric molecules, whereby a level crossing occurs between the energy levels of the ground and the excited states when the electric field of the laser pulse is antiparallel with the permanent dipole of the molecule ($\phi=0$). This level crossing leads to a strong population of the excited states, which in turn boosts EI.

This mechanism also nicely explains the sensitivity of EI and EE for other values of the CEP, as well as the fact that the strength of these CEP effects increases for increasingly short pulses and decreases with increasing laser pulse duration. We have also proposed a semiclassical nonadiabatic model, which explains the level crossing mechanism, and yields the internuclear distance at with EI, EE, and the energy level crossing occurs with good accuracy.

The strong nuclear charge asymmetry in HeH^{2+} leads to an unstable ground state, so that HeH^{2+} is quite different from realistic molecules which usually have a weaker charge asymmetry and which can possibly be used in experiments. To account for this, we performed simulations by assigning non-integer effective charges to the nuclei, leading to a weaker charge asymmetry. The results show that the sensitivity of EI to the laser CEP remains strong even for nonsymmetric molecules with a very weak charge asymmetry. This indicates that the nonsymmetric distribution of the electron cloud among the nuclei is critically responsible for the CEP sensitivity of EI.

The strong orientation and CEP dependence of EI as shown in the present simulations for one-electron nonsymmetric molecular systems could find applications in the control of the ionization of complex molecules [32], in the laser assisted population inversion in heavy ion collisions for x-ray laser production [33], and finally in the imprinting of nanostructures in heteroatomic lattices with ultrashort intense few cycle pulses [34].

ACKNOWLEDGMENTS

We thank the Natural Sciences and Engineering Research Council of Canada (NSERC) and the Canadian Institute for Photonics Innovation (CIPI) for their financial support.

[1] T. Zuo and A. D. Bandrauk, Phys. Rev. A **52**, R2511 (1995); T. Zuo, S. Chelkowski, and A. D. Bandrauk, *ibid.* **48**, 3837 (1993).
[2] T. Seideman, M. Y. Ivanov, and P. B. Corkum, Phys. Rev. Lett. **75**, 2819 (1995).
[3] K. Codling, L. J. Frasinski, and P. A. Hatherly, J. Phys. B **22**, L321 (1989); K. Codling and L. J. Frasinski, *ibid.* **26**, 783 (1993).
[4] S. Chelkowski and A. D. Bandrauk, J. Phys. B **28**, L723 (1995).
[5] *Molecules in Laser Fields*, edited by A.D. Bandrauk (Dekker, New York, 1994).
[6] M. Schmidt, D. Normand, and C. Cornaggia, Phys. Rev. A **50**, 5037 (1994); D. Normand and M. Schmidt, *ibid.* **53**, R1958 (1996).
[7] D. Pavičić, A. Kiess, T. W. Hänsch, and H. Figger, Phys. Rev. Lett. **94**, 163002 (2005).
[8] E. Constant, H. Stapelfeldt, and P. B. Corkum, Phys. Rev. Lett. **76**, 4140 (1996).
[9] G. N. Gibson, M. Li, C. Guo, and J. Neira, Phys. Rev. Lett. **79**, 2022 (1997).
[10] G. Lagmago Kamta and A. D. Bandrauk, Phys. Rev. A **75**, 041401(R) (2007).
[11] A. Hishikawa, A. Iwamae, and K. Yamanouchi, Phys. Rev. Lett. **83**, 1127 (1999).
[12] V. Veniard, R. Taieb, and A. Maquet, Phys. Rev. A **65**, 013202 (2001).
[13] C. Siedschlag and J. M. Rost, Phys. Rev. Lett. **89**, 173401 (2002); Phys. Rev. A **67**, 013404 (2003).
[14] M. Y. Shverdin, D. R. Walker, D. D. Yavuz, G. Y. Yin, and S. E. Harris, Phys. Rev. Lett. **94**, 033904 (2005).
[15] S. Chelkowski, P. B. Corkum, and A. D. Bandrauk, Phys. Rev. Lett. **82**, 3416 (1999).
[16] G. Lagmago Kamta and A. D. Bandrauk, Phys. Rev. Lett. **94**, 203003 (2005).
[17] T. Kirchner, Phys. Rev. Lett. **89**, 093203 (2002).
[18] I. Ben-Itzhak, I. Gertner, O. Heber, and B. Rosner, Phys. Rev. Lett. **71**, 1347 (1993).
[19] I. Ben-Itzhak, Z. Chen, B. D. Esry, I. Gertner, O. Heber, C. D. Lin, and B. Rosner, Phys. Rev. A **49**, 1774 (1994).
[20] I. Ben-Itzhak, J. P. Bouhnik, B. D. Esry, I. Gertner, O. Heber, and B. Rosner, Phys. Rev. A **54**, 474 (1996).
[21] G. Lagmago Kamta, A. D. Bandrauk, and P. B. Corkum, J. Phys. B **38**, L339 (2005).
[22] G. Lagmago Kamta and A. D. Bandrauk, Phys. Rev. A **71**, 053407 (2005).
[23] M. G. Baik, M. Pont, and R. Shakeshaft, Phys. Rev. A **54**, 1570 (1996).
[24] G. Lagmago Kamta and A.D. Bandrauk, Phys. Rev. A **70**, 011404(R) (2004).
[25] G. Lagmago Kamta and A. D. Bandrauk, Laser Phys. **15**, 502 (2005).
[26] P. Froelich, K. Szalewicz, B. Jeziorski, W. Kolos, and H. J. Monkhorst, J. Phys. B **20**, 6173 (1987).
[27] W. H. Press, S. A. Teukolski, W. T. Vetterling, and B. P. Flannery, *Numerical Recipes in Fortran: The Art of Scientific Computing*, 2nd ed. (Cambridge University Press, Cambridge, 1992).
[28] D. R. Bates and T. R. Carson, Proc. R. Soc. London, Ser. A **234**, 207 (1956).
[29] T. G. Winter, M. D. Duncan, and N. F. Lane, J. Phys. B **10**, 285 (1977).
[30] Z. Mulyukov, M. Pont, and R. Shakeshaft, Phys. Rev. A **54**, 4299 (1996); Z. Mulyukov and R. Shakeshaft, *ibid.* **63**, 053404 (2001).
[31] P. Dietrich and P. B. Corkum, J. Chem. Phys. **97**, 3187 (1992).
[32] Y. Sato, H. Kono, S. Koseki, and Y. Fujimura, J. Am. Chem. Soc. **125**, 8019 (2003).
[33] Y. Nagata, K. Midorikawa, S. Kubodera, M. Obara, H. Tashiro, and K. Toyoda, Phys. Rev. Lett. **71**, 3774 (1993).
[34] L. N. Gaier, M. Lein, M. I. Stockman, G. L. Yudin, P. B. Corkum, M. Y. Ivanov, and P. L. Knight, J. Mod. Opt. **52**, 1019 (2005).